Effect of Annealing on the Structure of Injection-Molded Pen

Y. ÜLÇER and M. CAKMAK*

Polymer Engineering Institute, College of Polymer Engineering and Polymer Science, The University of Akron, Akron, Ohio 44325-0301

SYNOPSIS

The influence of annealing at temperatures where thermally activated crystallization rates become significant on the structural variations in the injection-molded polyethylene naphthalate (PEN) was investigated. In these studies, two distinct shear crystallized layers are observed. The shear crystallized layer near the skin forms during the filling stage, and the second shear crystallized layer forms during the packing stage but remains optically unobservable until the annealing takes place. Upon annealing, additional layers with larger crystallite sizes form around these preformed highly oriented layers. The α and β phases were observed in both of the shear crystallized layers. The β phase is generally grown either under high deformation fields or under quiescent conditions at high temperatures. © 1996 John Wiley & Sons, Inc.

INTRODUCTION

Recent studies[1-5] showed that both stress and temperature are effective in determining the final crystallinity distribution in injection molded slowly crystallizing polymers. The crystallinity increase brought up by an increase in the mold temperature is usually accompanied by a loss of preferential orientation developed during the filling stage. This is generally attributed to the reduction of stress history by a decrease in viscosity and to the increase in the rate of orientation relaxation with increasing temperature.

In a previous paper,[5] we showed that the thermal crystallization of polyethylene naphthalate (PEN) through the use of high mold temperatures requires holding times exceeding 10 min due to its very slow crystallization kinetics.[6] This value is well above the industrially feasible cycle times. Early studies of the crystallization kinetics of slowly crystallizing polymers[7] showed that, even in the absence of stress effects, the nucleation density of the quenched samples are highly enhanced due to the self seeding phenomenon. The extra nuclei responsible for the self seeding are created during the cooling stage, but their growth is hampered by the rapid drop in the temperature of the surroundings. On the other hand, the structural study of injection-molded s-PS[8] and stress-induced crystallization studies[9,10] showed that, if quenching is accompanied by flow, the energy barrier to form a nuclei is greatly reduced as a result of preferential chain orientation, increasing their number significantly. In this paper, it is our aim to show that a combination of self seeded and oriented nuclei are present in the "apparently" amorphous core of injection molded PEN. Thus, annealing the samples molded at low mold temperatures will not only enhance the crystallization kinetics of PEN but also result in structural gradients that are unique and quite different from the as-molded samples.

EXPERIMENTAL

Material

PEN used in this study was provided by Goodyear Co. under the trade name Traytuf HP, VFR40008X. It is an injection molding grade PEN, having an intrinsic viscosity of 0.824 dL/g. The PEN pellets

* To whom correspondence should be addressed.

Journal of Applied Polymer Science, Vol. 62, 1661-1678 (1996)
 CCC 0021-8995/96/101661-18

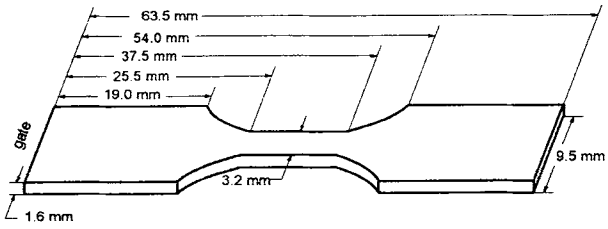

a)

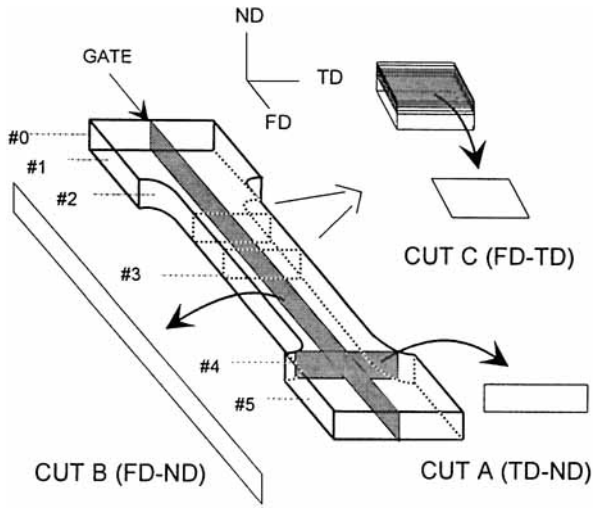

b)

Figure 1 Dimensions of the cavity and the cutting procedures.

were dried in a vacuum oven at 145°C for at least 24 h. and processed immediately after drying.

Injection Molding

End-gated ASTM small dumbbells were injection molded at mold temperatures of 20, 90, and 120°C using a Boy 15S injection molding machine. Two injection speeds corresponding to 5.00 cm/s, (high) and 2.10 cm/s (low) were used. All the other molding conditions were the same as Ülçer and Cakmak.[5]

After molding, the injection molded parts were attached to a metal frame that was inserted to a forced convection annealing chamber. The oven's temperature was kept at 160 ± 0.5°C. The annealing times varied between 5 and 25 min.

Cutting Procedures

In order to characterize the internal structure of the injection molded dumbbells, sectioning procedures A and B, described in Ülçer and Cakmak[5] were used (Figure 1). Procedure A involved cutting sections of ca. 0.6 mm thickness perpendicular to the flow direction in the transverse direction–normal direction (TD–ND) plane. Procedure B consisted of cutting a slice along the centerline of the specimen in the flow direction–normal direction (FD–ND) plane.

Optical Microscopy

The transmission optical photomicrographs of the samples were obtained by using the A and B cuts as negatives in a photographic enlarger.

Hot-stage Microscopy

A B-cut sample microtomed from location 3 of a small dumbbell was inserted between thin cover glasses and placed in a Mettler FP82 HT hot stage. The hot stage was placed on a Leitz Laborlux 12S POL polarized microscope such that the FD of the sample makes an angle of 45 degrees to the crossed polars. The sample was heated with 10°C/min heating rate in the temperature range of 50 to 310°C. The heating and melting sequence was recorded using a Sony 3 CCD camera connected to both a video recorder and the image capturing card of a Sun 4/150 workstation. The differential scanning calorimetry (DSC) scan of the same sample was acquired in a Perkin Elmer DSC model 7 using a heating rate of 10°C/min.

Wide-angle X-ray Diffraction Through Matrixing Microbeam Camera

Using the matrixing microbeam X-ray (MMBX) camera developed in our laboratories, a series of WAXS patterns were obtained at regular intervals from skin to core at selected locations along the flow direction. The B-cut samples were mounted on the precision X-Y stage of the MMBX with X-ray beam normal to the FD-ND plane (Figure 2). The MMBX camera was connected to a Rigaku RU-200B rotating anode X-ray generator that was operated at 40 kV and 150 mA. The X-ray beam was collimated to 100 μm using a pinhole collimator and monochromatized using a nickel foil filter in order to obtain CuKα radiation (λ = 1.542 Å).

Small-angle X-ray Scattering

Small-angle X-ray scattering (SAXS) patterns of the selected samples were taken at the University of Hamburg DESY Synchrotron Radiation source. The crystalline regions of the B-cuts taken from selected samples were separated and placed in the

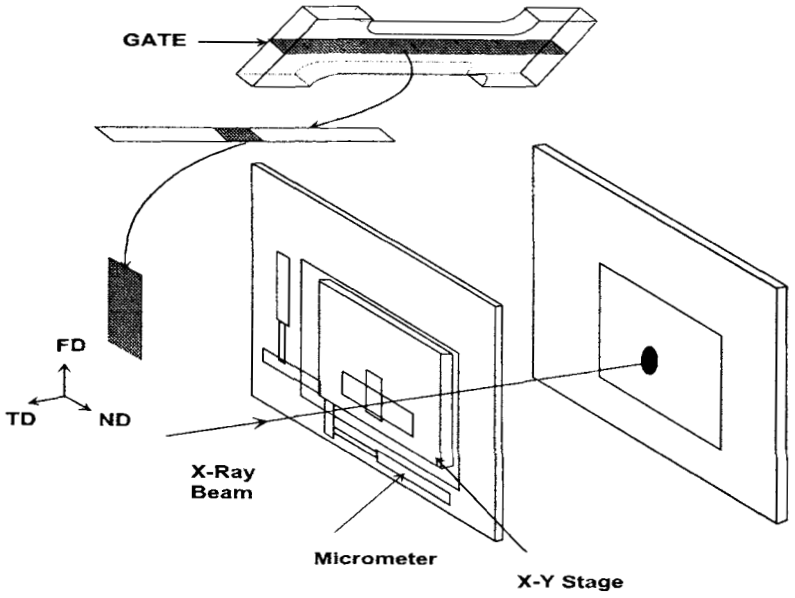

Figure 2 Diagram showing the mounting of the B cut samples to the X-Y stage of the microbeam X-ray camera and the direction of the X-ray beam.

vacuum chamber connecting the collimated beam to the two-dimensional wire detector (Figure 3). The incoming beam was monochromatized to 1.54 Å. The sample-to-film distance was 224.5 cm.

RESULTS

Optical Microscopy

The structural studies we carried out earlier on injection molded PEN[5] showed that PEN exhibits a three-layer structural gradient consisting of an amorphous skin, a shear crystallized intermediate layer, and an amorphous core, at mold temperatures up to its glass transition temperature (Figs. 4 and 5). In general, the crystalline regions of PEN are opaque, whereas the transparent portions are amorphous. This is not entirely true for all of this class of slow crystallizing polymers; but for PEN, this behavior was found to be prevalent.

In order to show the structural variations in annealed samples, diamond saw cut sections were taken from various regions of the molded parts. These were used as negatives to obtain enlarged prints. On these prints, the regions, which are opaque, do not transmit light and appear as bright regions. The regions that are transparent transmit light and, as a result, appear dark.

The morphology of the annealed samples was found to be quite different from the three-layer morphology of the as-molded samples. In order to describe the complex structural gradients observed in the annealed samples, we labeled all the layers in the order of appearance from skin to core (Figure 6).

Figure 7(a) shows sections cut in the ND-TD plane (cut A) of a sample molded at 20°C using the low injection speed and, subsequently, annealed at

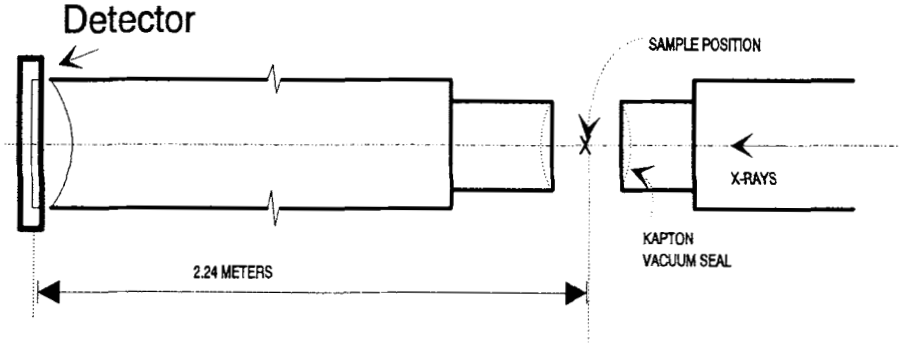

Figure 3 Schematics of the synchrotron beam line used in SAXS study.

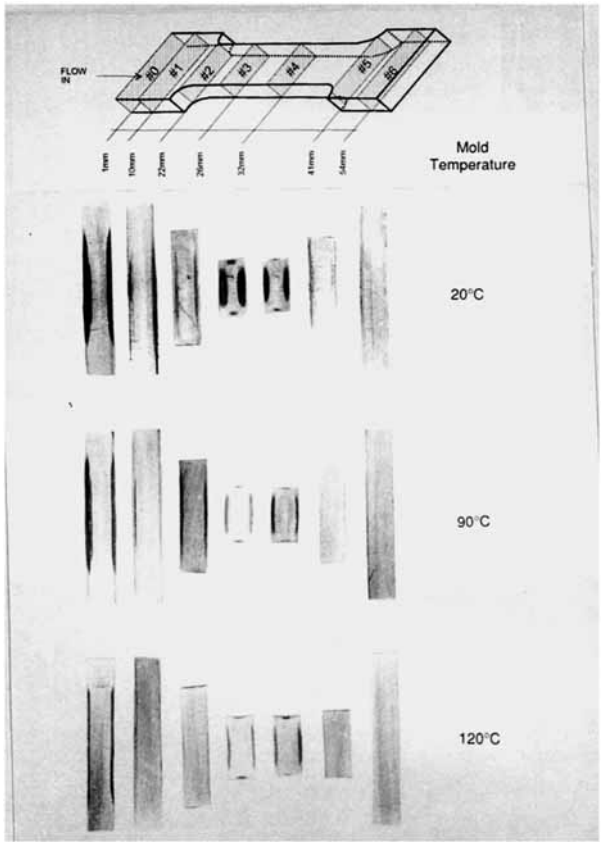

Figure 4 Transmission optical photomicrographs of A cuts taken from the indicated locations of samples molded using the low injection speed.

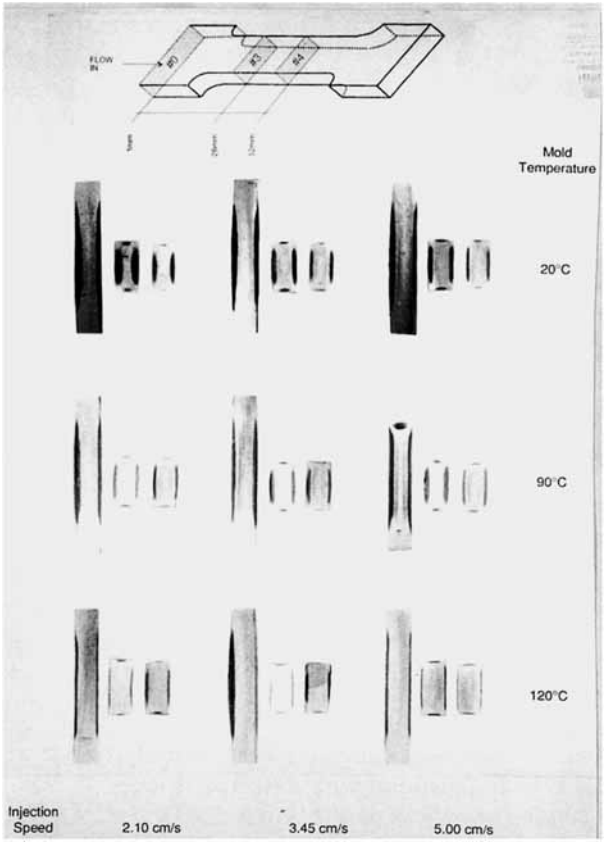

Figure 5 Transmission optical photomicrographs showing the effect of mold temperature and injection speed on the structure of the A cuts taken from the indicated regions.

160°C for 7 min. In this cut plane, we observe an opaque crystalline layer (layer 2 in Fig. 6) near the skin. This layer extends like a strip and covers most of the four broad surfaces of the samples in all locations except at the four corners and at the end of the cavity (location 6). Referring back to the optical photomicrographs of as-molded samples (Figs. 4 and 5), we noticed that this layer has the same features as the shear crystallized layers that formed during the filling stage, as follows: (1) it disappears at the four corners where the stress history is the lowest; (2) its thickness increases at locations where the deformation history is maximum (locations 0, 3, and 4 in the flow direction and middle of the transverse direction); (3) at locations 2, 3, and 4, it can be seen next to all four surfaces. After annealing, this layer becomes visible, even at locations where shear crystallized layers were not clearly visible in the as-molded samples, namely, locations 1 and 6. Also, in the annealed samples, the shear crystallized layer was surrounded by a more opaque crystalline ring (layer 1 in Fig. 6). Beneath the shear crystallized layer, we observe a second opaque layer that was not visible in the as-molded samples (layer 4 in Fig. 6). It also extends like a strip, but the length of the strip in the TD is narrower than the shear crystallized layer. As with the shear crystallized layer, it is surrounded by a more opaque crystalline ring (layer 3). The thickness of this second crystalline layer also increases at locations subjected to high deformations (locations 0, 3, and 4). Likewise, at these locations, the spacing between the two crystalline

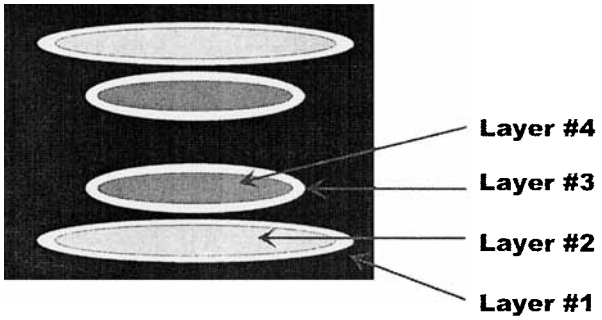

Figure 6 Schematics of the structural gradients observed in the ND-TD plane (cutting procedure A).

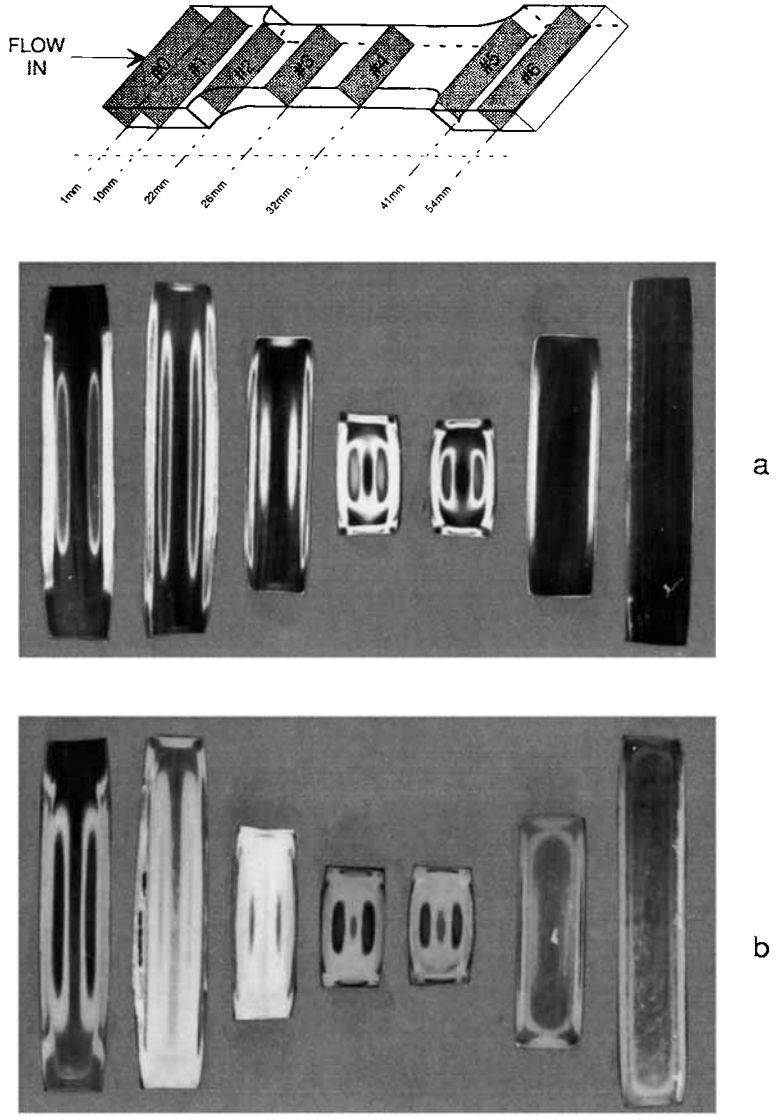

Figure 7 Transmission optical photomicrographs of the A cuts taken from the indicated locations of a sample molded at a mold temperature of 20°C using the low injection speed. The sample was crystallized for (a) 7 and (b) 15 min.

layers (layers 2 and 4) decreases and is covered by the dark opaque crystalline layers (layers 1 and 3) that separate them, merging the two layers. These observations indicate that the formation of layer 4 is also related to the stress field caused by the flow. Unlike the first shear crystallized layer, which covers all the four surfaces, the second shear crystallized layer (layer 4) was seen only near the two broad surfaces of the moldings. The translucent characteristic of this layer suggests that the size of the crystals forming it is smaller than those that form the shear crystallized layer near the skin. These two layers will be referred to as first and second shear crystallized layers, respectively. Finally, the core of the sample consists of transparent amorphous regions that appear dark in these pictures.

The effects of increasing annealing time can be seen in Figure 7(b), where the A cuts taken from a sample molded at 20°C and annealed for 15 min are shown. Increasing the annealing time does not change the appearance and thickness of the two shear crystallized layers observed in Figure 7(a) (layers 2 and 4); yet it increases the thickness of the opaque rings that surround them (layers 1 and 3). These opaque layers consist of larger crystallites, whose sizes are on the order of the visible light; and they are formed in the regions where the polymer melt was subjected to lower deformation history. The

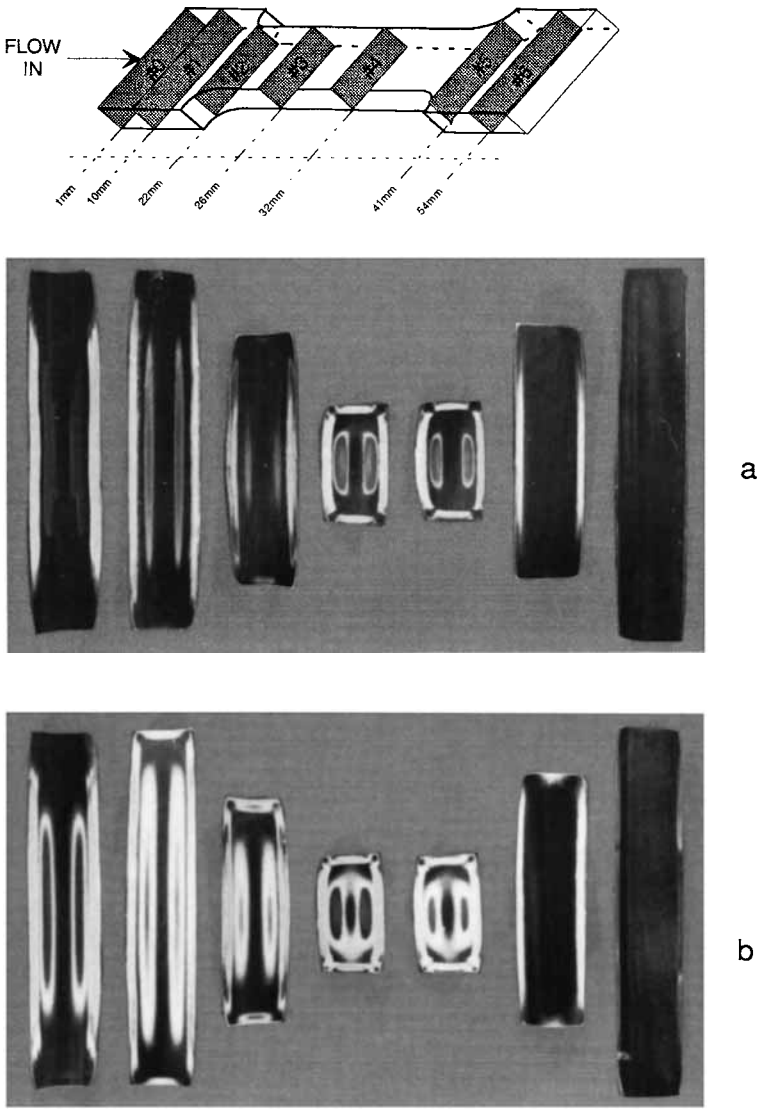

Figure 8 Transmission optical photomicrographs of the A cuts taken from the indicated locations of a sample molded at a mold temperature of 20°C using the high injection speed. The sample was crystallized for (a) 7 and (b) 15 min.

crystallites that form under such conditions are larger in size due to the decrease in nucleation density in the absence of large frozen in orientations. These regions constitute the transition regions between the translucent high shear crystallized regions and the transparent core. When sufficient thermal energy is provided, the boundary between this opaque region and the amorphous region expands into amorphous region, covering most of the amorphous core.

Increasing the annealing time reveals several new features at locations 5 and 6. Near the skin of location 6, we could now observe two opaque layers (layers 1 and 2) that were not visible in the samples annealed for shorter periods. Also, at the center of these locations, several concentric rings, reminiscent of the ones observed at the end region of injection molded s-PS,[8] become visible.

The effect of increasing injection speed can be seen in Figure 8, where the transmission optical photomicrographs of a sample molded at 20°C using the high injection speed and subsequently annealed at 160°C are presented. After 7 min annealing time [Fig. 8(a)], we observe that the thickness of both the first and second shear crystallized layers (layers 2 and 4) are decreased. However, the change in the thickness of dark opaque ring that surround the second shear crystallized layer (layer 3) is more pro-

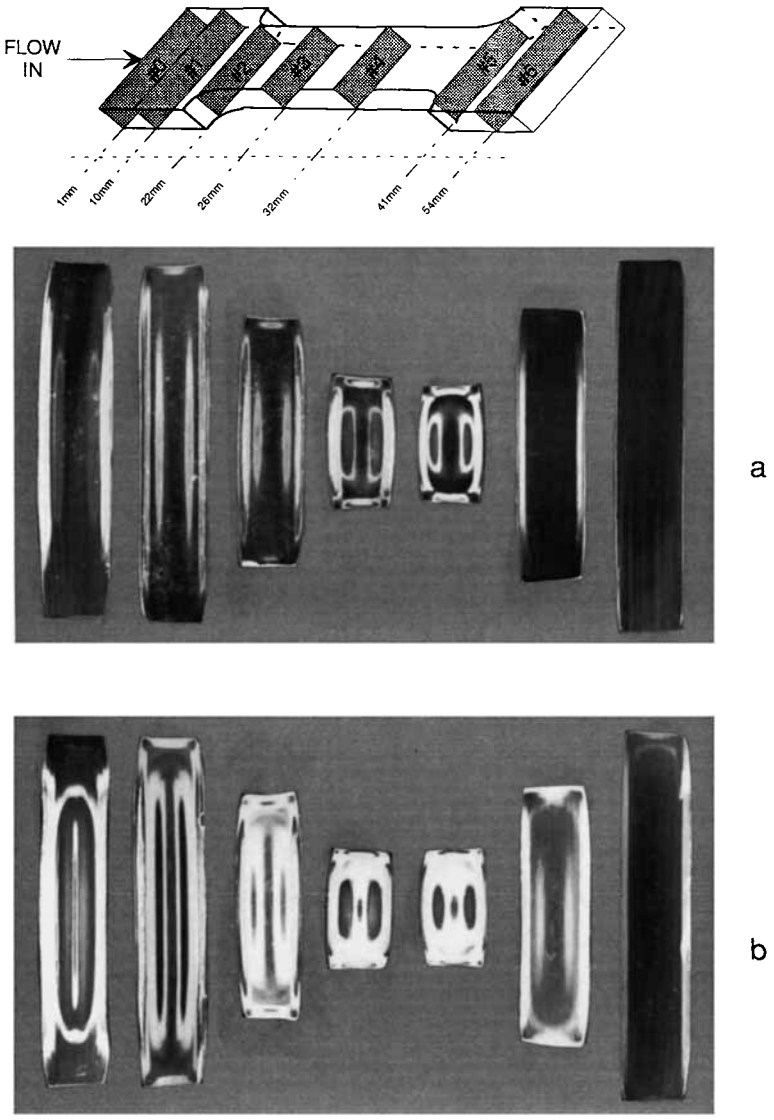

Figure 9 Transmission optical photomicrographs of the A cuts taken from the indicated locations of a sample molded at a mold temperature of 90°C using the low injection speed. The sample was crystallized for (a) 7 and (b) 15 min.

nounced. This was attributed to the decrease in the stress history in these regions: When the injection speed increases, the cavity is filled much faster. As a result, the time during which the melt is in contact with the cold cavity walls is reduced, and the overall melt temperature increases. This has two effects: (1) the viscosity of the melt is reduced, and (2) the thickness of the frozen layer decreases (or the available cross-sectional area of the flow channel increases); both reduce the stress history.

When the samples molded with high injection speed are annealed for 15 min. [Fig. 8(b)], the thickness of dark opaque rings (layers 1 and 3) that surround the shear crystallized layers increases. However, this increase is less pronounced than the samples molded at the low speed. As a result, the dark opaque layers cannot totally cover the core of the samples, and transparent amorphous regions can still be observed at the end of the mold. Note that the increase in the thickness of the first dark opaque layer (layer 1) is limited since it is sandwiched between the skin and the second dark opaque ring (layer 3).

The effects of mold temperature and injection speed on the structural gradients are shown in Figures 9–12. In general, the thickness of the first and second shear crystalline layers (layers 2 and 4) slightly decreases with increasing mold temperature.

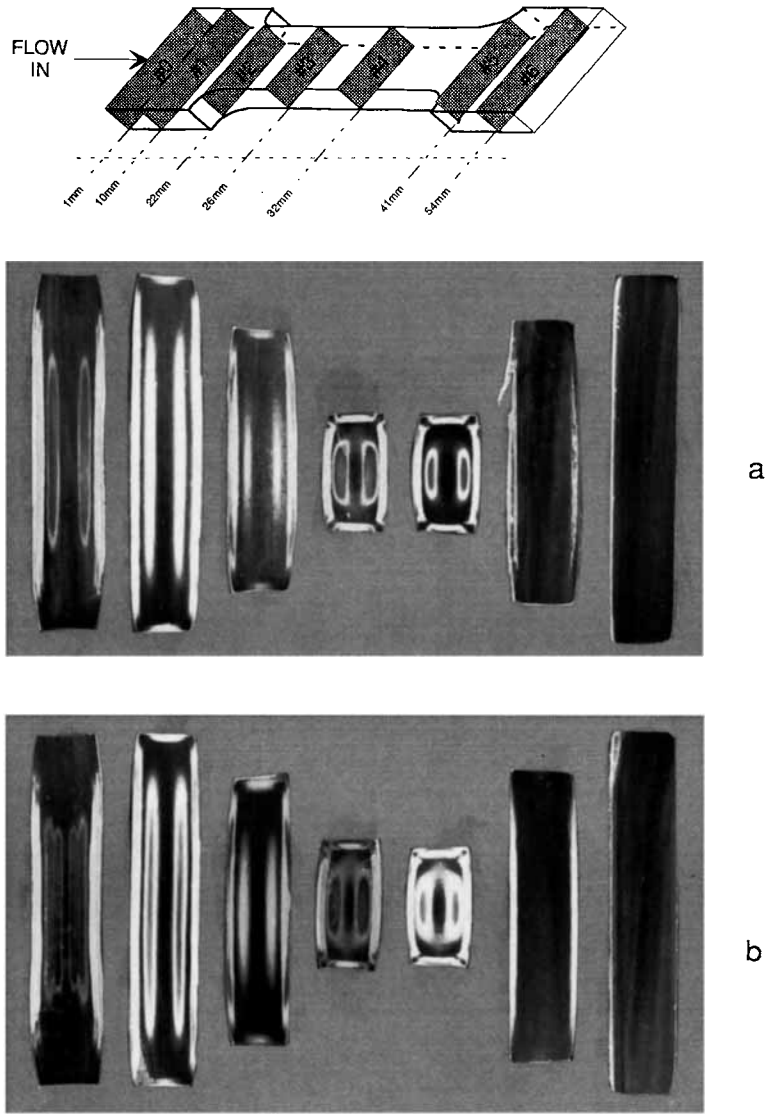

Figure 10 Transmission optical photomicrographs of the A cuts taken from the indicated locations of a sample molded at a mold temperature of 90°C using the high injection speed. The sample was crystallized for (a) 7 and (b) 15 min.

The thickness of the second dark opaque layer (layer 3), on the other hand, decreases significantly. As a result, the core of the samples molded at 120°C and low injection speed remains mainly transparent (amorphous), and the concentric rings are not visible even after annealing for 15 min (Fig. 11).

The decrease in the thickness of opaque regions (layers 1 and 3; thus the degree of crystallinity) is more prominent in the samples molded with high injection speed. Especially in the sample molded at 120°C using the high injection speed, the second shear crystalline layer (layer 4) is not visible at locations 0 and 1 (gate region) unless it is annealed for 15 min (Fig. 12). We also noticed that at the entrance of the cavity (location 1) in the samples molded with low injection speed, the second shear crystallized layer (layer 4) approaches the core with increasing mold temperature.

Figures 13–15 show the B cuts taken from the annealed small dumbbells. Again, we can distinguish the first shear crystallized layer (layer 2) near the skin and the second shear crystallized layer (layer 4) near the core. In the FD-ND plane, we can clearly see that both layers 2 and 4 concentrate at locations where the stresses acting on the flowing melt are the highest (gate and neck

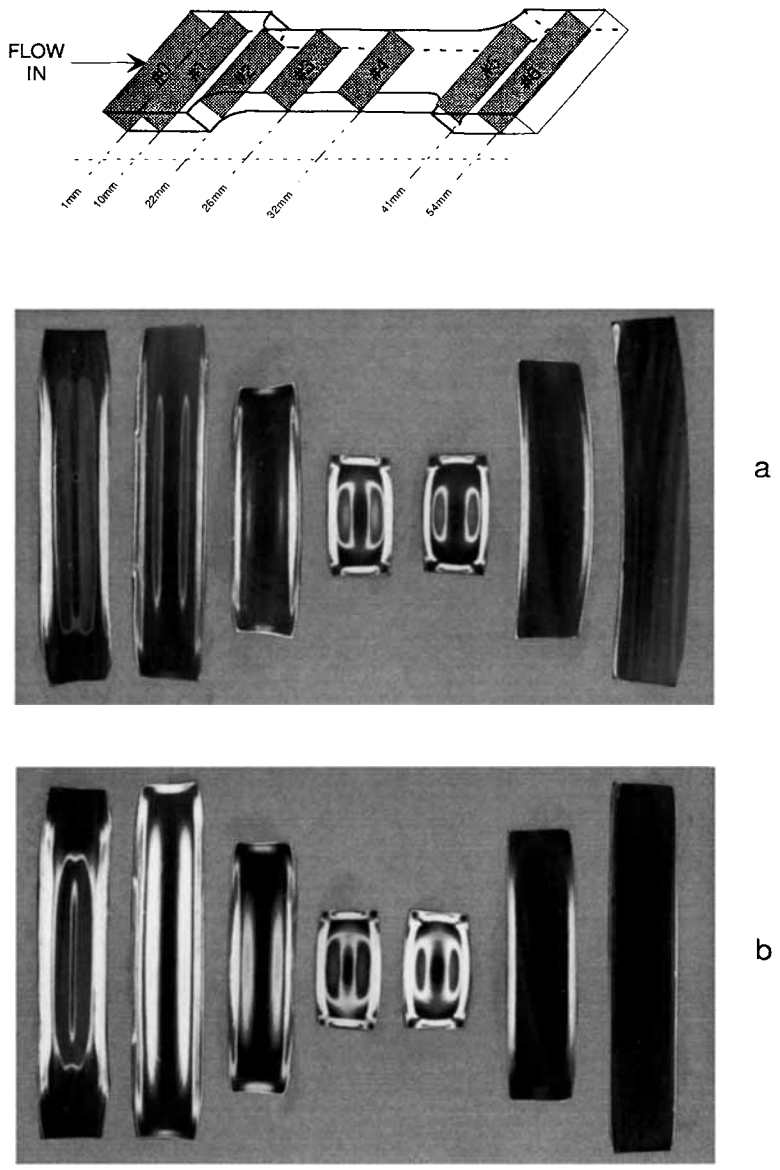

Figure 11 Transmission optical photomicrographs of the A cuts taken from the indicated locations of a sample molded at a mold temperature of 120°C using the low injection speed. The sample was crystallized for (a) 7 and (b) 15 min.

region). After annealing for 15 min, with the exception of the sample molded at 120°C, the core of the samples molded using the low injection speed becomes opaque, and the second shear crystallized layer becomes distinguishable due to its translucent character [Figs. 13(b) and 14(b)]. At the end region of the mold (locations 5 and 6) of these samples molded with low injection speed, we note several opaque crystalline layers. These correspond to the locations where the cutting plane (FD-ND) intersects the concentric rings observed in the ND-TD plane of the same samples [Figs. 7(b) and 9(b)]. In this plane, we can clearly see that increasing injection speed does not significantly affect layers 1, 2, and 4. Its main effect is to decrease the thickness of the dark crystalline layers (layer 3); thus, the overall crystallinity of the sample. Although it is not obvious in the A cuts, the B cuts show that, with increasing mold temperature, the second crystalline layer (layer 4) becomes broader and extends until the end of the diverging region (location 5).

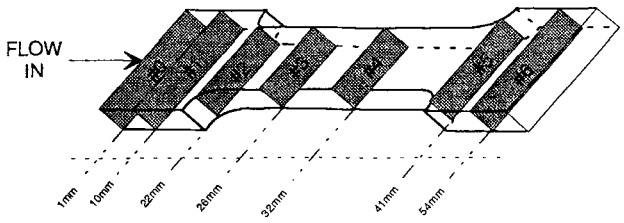

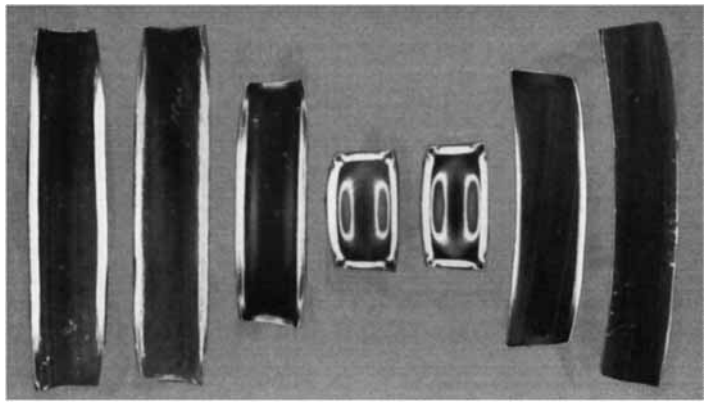

a

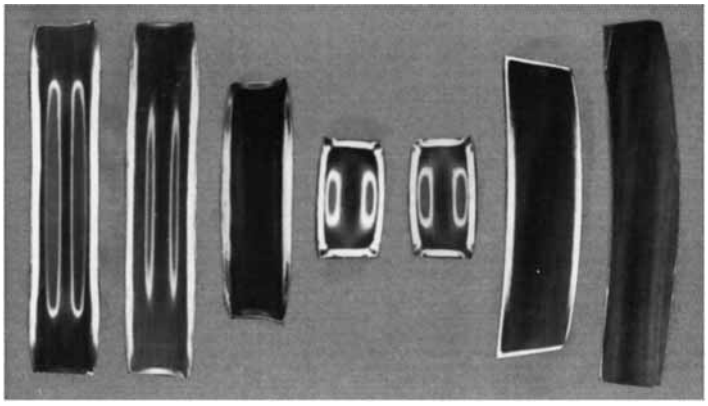

b

Figure 12 Transmission optical photomicrographs of the A cuts taken from the indicated locations of a sample molded at a mold temperature of 120°C using the high injection speed. The sample was crystallized for (a) 7 and (b) 15 min.

Hot-stage Melting

In our earlier paper,[5] we have shown that there was a distinct difference in the crystallization and melting behavior of amorphous and crystalline layers observed in injection molded PEN. In this section, the same approach was adopted in order to understand the origin of different layers observed in the annealed samples. A microtomed sample was placed at 45 degrees to the extinction axis of the polarizer and analyzer of the polarized microscope, and the intensity of the transmitted depolarized light was monitored.

Figure 16 shows optical photomicrographs taken during the melting sequence of a B cut taken from location 3 of a sample molded at the mold temperature of 20°C using the low injection speed and annealed for 7 min. Below the glass transition temperature (T_g = 120°C), we can identify the first shear crystallized layer (layer 2) near the skin. At location 3, the first and second dark opaque layers [layers 1 and 3] merge into one layer, which is re-

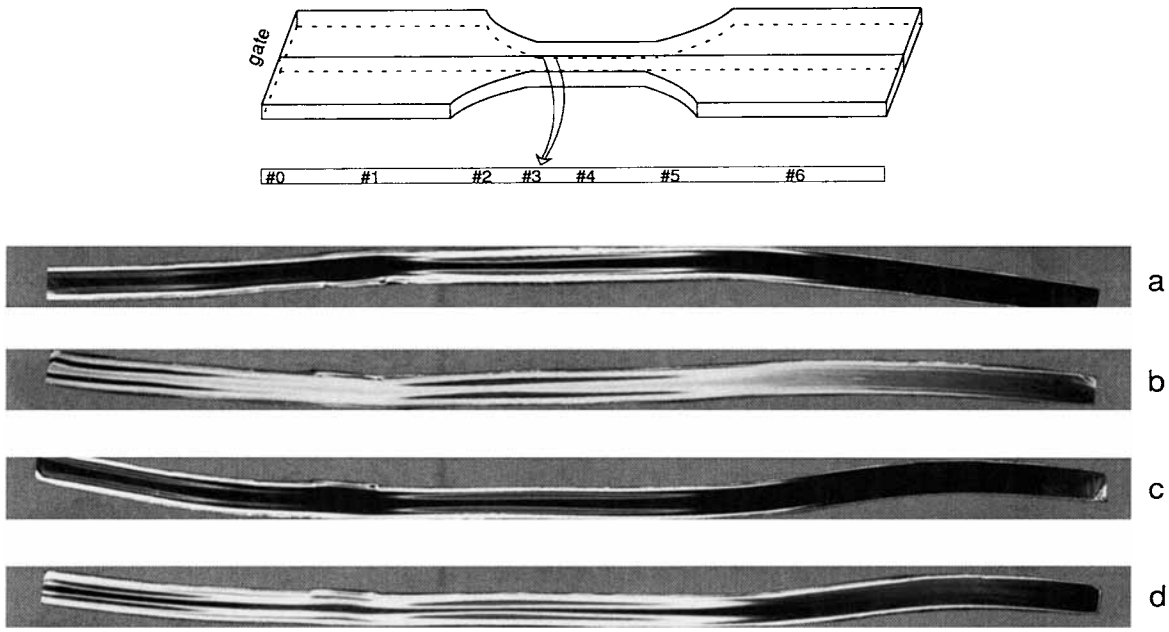

Figure 13 Transmission optical photomicrographs of the B cuts. Sample molded at a mold temperature of 20°C: low injection speed annealed for (a) 7 and (b) 15 min; high injection speed annealed for (c) 7 and (d) 15 min.

ferred to as the intermediate layer in Figure 16. Finally, at the core, we have the second dark opaque layer [layer 3].

At 70°C, the intermediate and core regions have a high light intensity compared to shear crystallized layers [layers 2 and 4], whose intensity was suppressed due to their relative opacity at this short annealing time. After the glass transition temperature of PEN (120°C) was reached, increasing segmental motion caused the light intensity of the in-

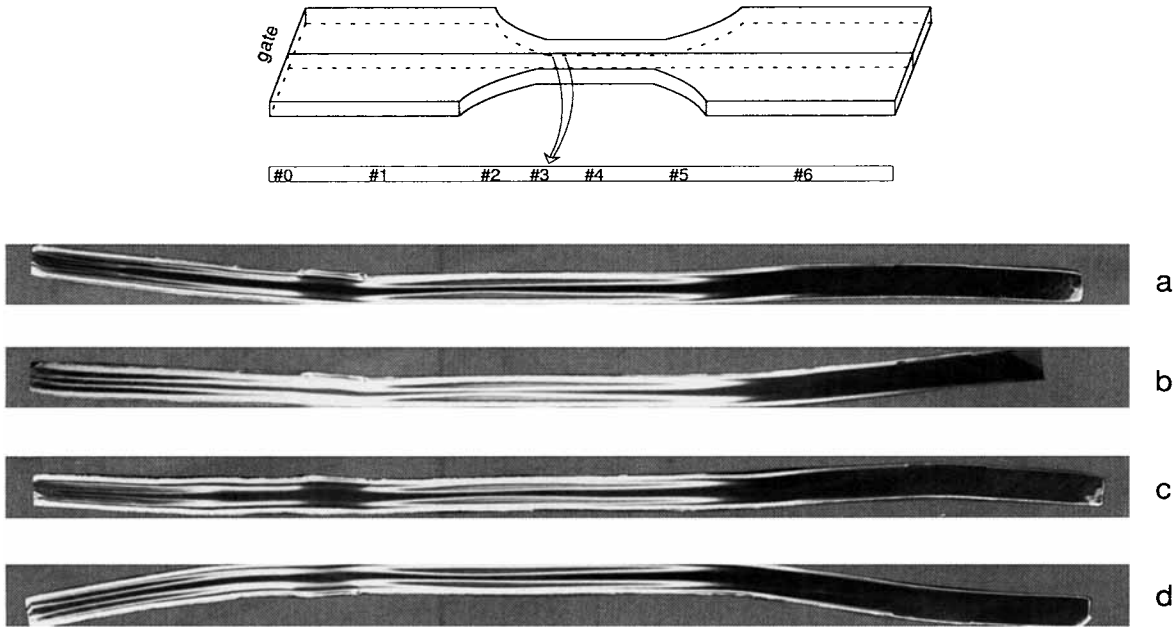

Figure 14 Transmission optical photomicrographs of the B cuts. Sample molded at a mold temperature of 90°C: low injection sped annealed for (a) 7 and (b) 15 min; high injection speed annealed for (c) 7 and (d) 15 min.

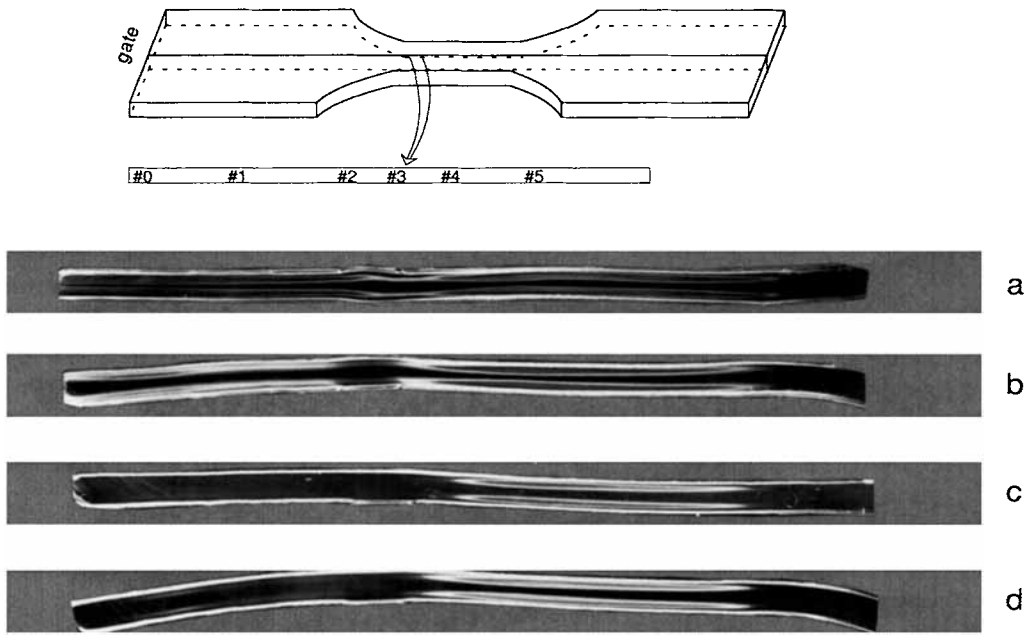

Figure 15 Transmission optical photomicrographs of the B cuts. Sample molded at a mold temperature of 120°C: low injection speed annealed for (a) 7 and (b) 15 min; high injection speed annealed for (c) 7 and (d) 15 min.

termediate and core regions to decrease. The fact that a change in the depolarized light intensity due to the segmental motion was still detectable suggest that the birefringence caused by the frozen stresses did not relax at this location of the of molding after 7 min of annealing.

Around 160°C, the depolarized light intensity of the intermediate and core regions reaches a minimum, allowing us to distinguish the dark crystalline layers that surround the shear crystallized layers. At 160°C, which marks the onset of cold crystallization, the crystallinity of the intermediate and core region slowly starts to increase as marked by an increase in the opacity of this region. The increase in the crystallization is almost complete around 220°C. As the temperature approaches 260°C, the thermally crystallized regions starts to mel, and the shear crystallized layers can clearly be distinguished. The second shear crystallized layer (layer 4) begins to melt around 270°C. The melting starts from the outer edges of the crystalline layers and proceeds inwards. At 295°C, the melting of the second shear region is complete. Like the shear crystallized layers in the as-molded samples,[5] the first shear crystallized layer (layer 2) melts around 300°C. The DSC scans of the same location (3) did not show a distinct melting peak around 290°C (Fig. 17), which corresponds to the melting point of the secondary shear crystallized layer. This clearly indicates that the depolarized light intensity is more sensitive to the transitions that take place during heating experiments.

Microbeam WAXS

Typical WAXS patterns obtained from the shear crystallized region of an as-molded and subsequently annealed sample are compared in Figure 18. We can see that both crystallinity and order of the sample that was molded at 20°C can be improved by annealing it. The diffraction peaks corresponding to the α-form of PEN were indexed according to d-spacing of the planes experimentally indexed by Mencik.[11] The β-form planes, on the other hand, were indexed according to the d-spacing values calculated from the unit cell dimensions that were reported by Buchner et al.[12] However, there were two peaks at the respective 2τ angles of 16.02 and 42.90 degrees that could not be indexed. This latter peak was also observed by Cakmak and Kim[13] after annealing melt spun fibers that showed the presence of β crystals. These peaks can be associated with the β-form, whose detailed crystallographic analysis and accurate the unit cell parameters are currently lacking.

MMBX WAXS experiments were carried out in order to determine the orientation and crystal form of different layers observed in the annealed samples.

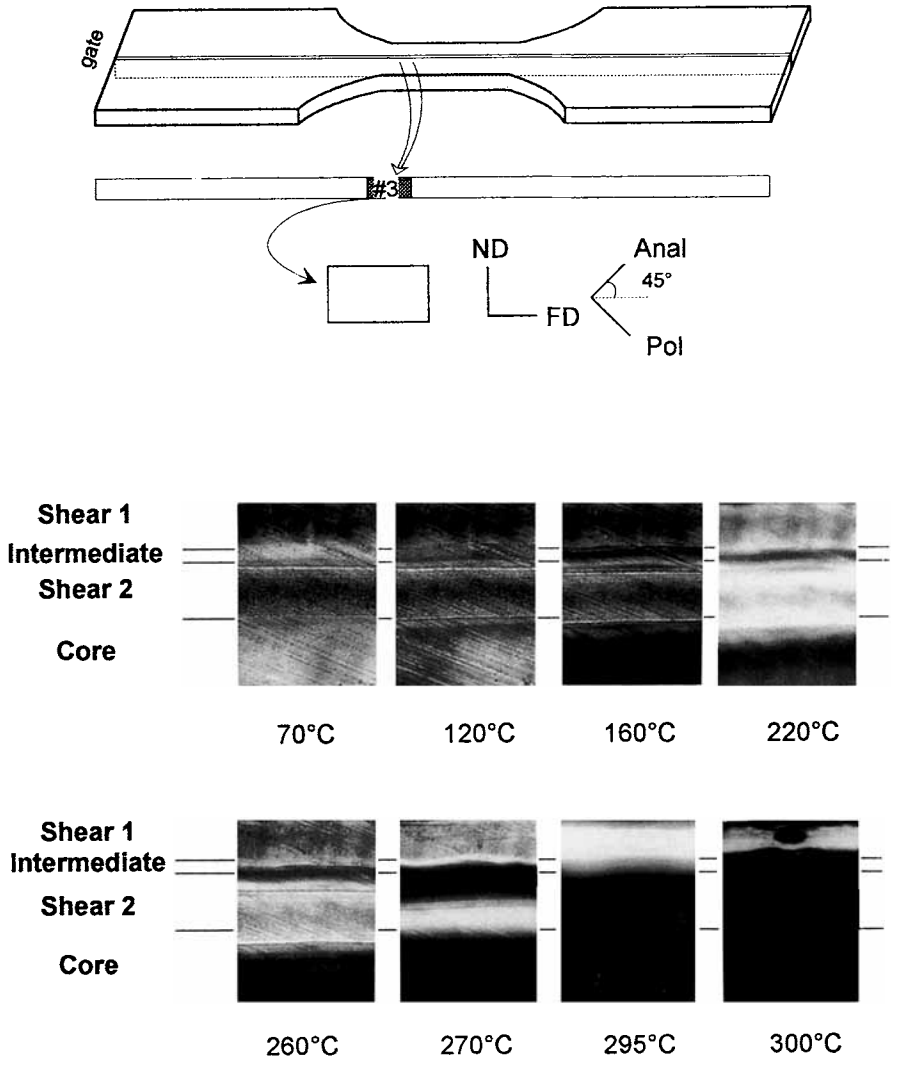

Figure 16 Melting sequence of a B cut taken from location 3 of a sample molded at a mold temperature of 20°C using the low injection speed. Annealing time: 7 min.

Figure 19 shows the skin to core MMBX WAXD patterns of the location 3 of B cuts taken from samples molded at a mold temperature of 20°C and subsequently annealed for 15 min. At the skin region of the sample (50–250 μm, layer 2) that was molded using the low injection speed [Fig. 19(a)], we observe highly oriented WAXS patterns similar to those observed in the shear crystallized layers of as-molded samples. The presence of strong diffraction peaks belonging to (010), (100), and (110) α planes as well as the (020) and (111) β planes indicates the presence of a mixture of α and β crystals. Moreover, the presence of several peaks at all layers indicates that the three-dimensional order is established in the shear crystallized region of this sample.

The WAXS patterns of the second shear crystallized layer (layer 4) (450–650 μm) show the same mixture of the α and β crystals; however, the orientation of this layer is lower, as indicated by the increasing azimuthal spread of the diffraction arcs. The local symmetry axis of the second shear crystallized layer is tilted towards the core about 15 degrees. The diffraction rings that were superposed onto the oriented diffraction arcs suggests the presence of an almost randomly oriented layer of α crystals [the (010) planes still show some preferred orientation] between the two shear crystallized layers (layers 1 and 3 merged together) (350 μm). Finally, at the core, we observe randomly oriented crystalline diffraction rings belonging to the α-form of PEN.

Combining these results with the transmission optical photomicrographs of the location 3, we concluded that the first shear crystalline layer

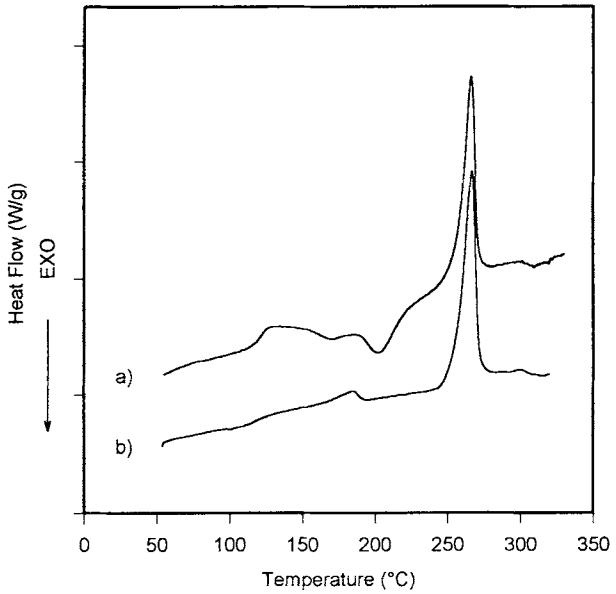

Figure 17 The DSC spectra of samples taken from location 3 of dumbbells molded at 20°C using the low injection speed. Annealing time: (a) 7 and (b) 15 min.

consists of a mixture of highly oriented α and β crystals. Similarly, the second shear crystalline layer consists of a mixture of α and β crystals, but these crystals are less oriented, and their local symmetry axes are tilted towards the core. Finally, the dark opaque rings (layers 1 and 3) that surround these shear crystallized layers consist of thermally induced and randomly oriented α-form crystals.

Increasing the injection speed does not significantly affect the characteristics of the shear crystallized layers [Fig. 16(b)]. Nevertheless, the thickness of the second shear crystallized layer (layer 4) slightly decreased with increasing injection speed. The reason for this reduction in shear crystallized thickness is due to reduction of stress history in the parts with increasing injection speed. In the samples molded with the low injection speed, we observe thicker shear crystallized layers because, in this sample, the solid-liquid boundary that evolve during the injection becomes much thicker during the course of filling since the flow front moves much more slowly than in higher injection speed. This causes larger fraction of the melt to be subjected to shearing and the largest stresses occur near the solid liquid boundary during the filling. This results in shear crystallization.

The effect of increasing the mold temperature can be seen in Figure 20, where the skin-to-core MMBX WAXS patterns of samples molded at a mold temperature of 120°C are presented. Again, the first shear crystallized layer (layer 2) showed highly oriented diffraction spots belonging to α and β crystal forms of PEN (0–150 μm); but as expected, its thickness decreased. The intermediate randomly oriented dark crystalline layers (layers 1 and 3 combined) also became thinner and could not be resolved separately since our beam size was limited to 100 μm. The tilted patterns characteristic of second shear crystallized layer (layer 4) covered most of the intermediate region from 250 to 550 μm, their thickness and orientation not being significantly affected by the increase in the mold temperature. At the end of second shear crystallized layer, we can distinguish the randomly oriented dark crystalline layers belong-

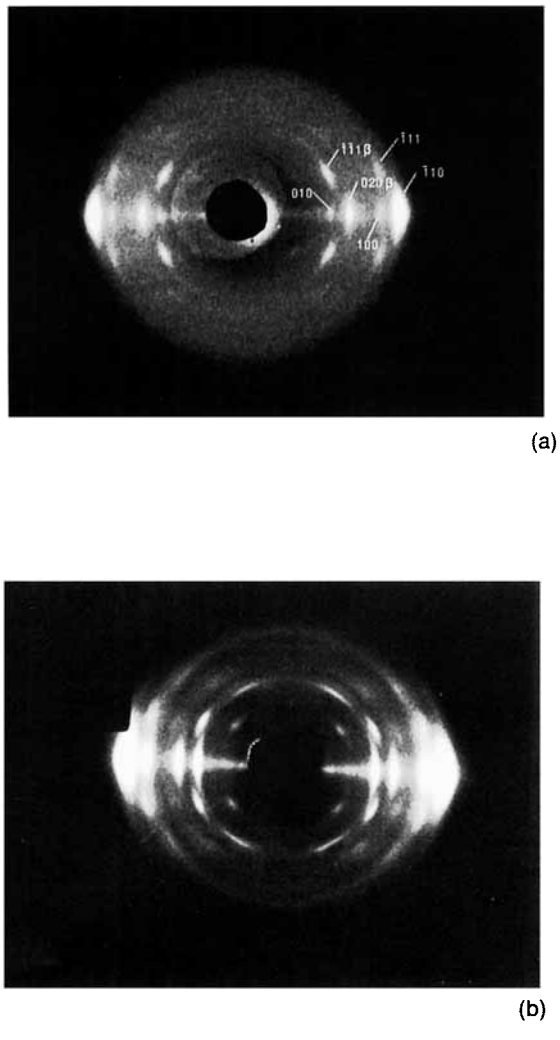

Figure 18 Typical WAXS patterns of the shear crystallized regions of a sample molded at 20°C using the low injection speed: (a) as-molded and (b) subsequently annealed for 15 min.

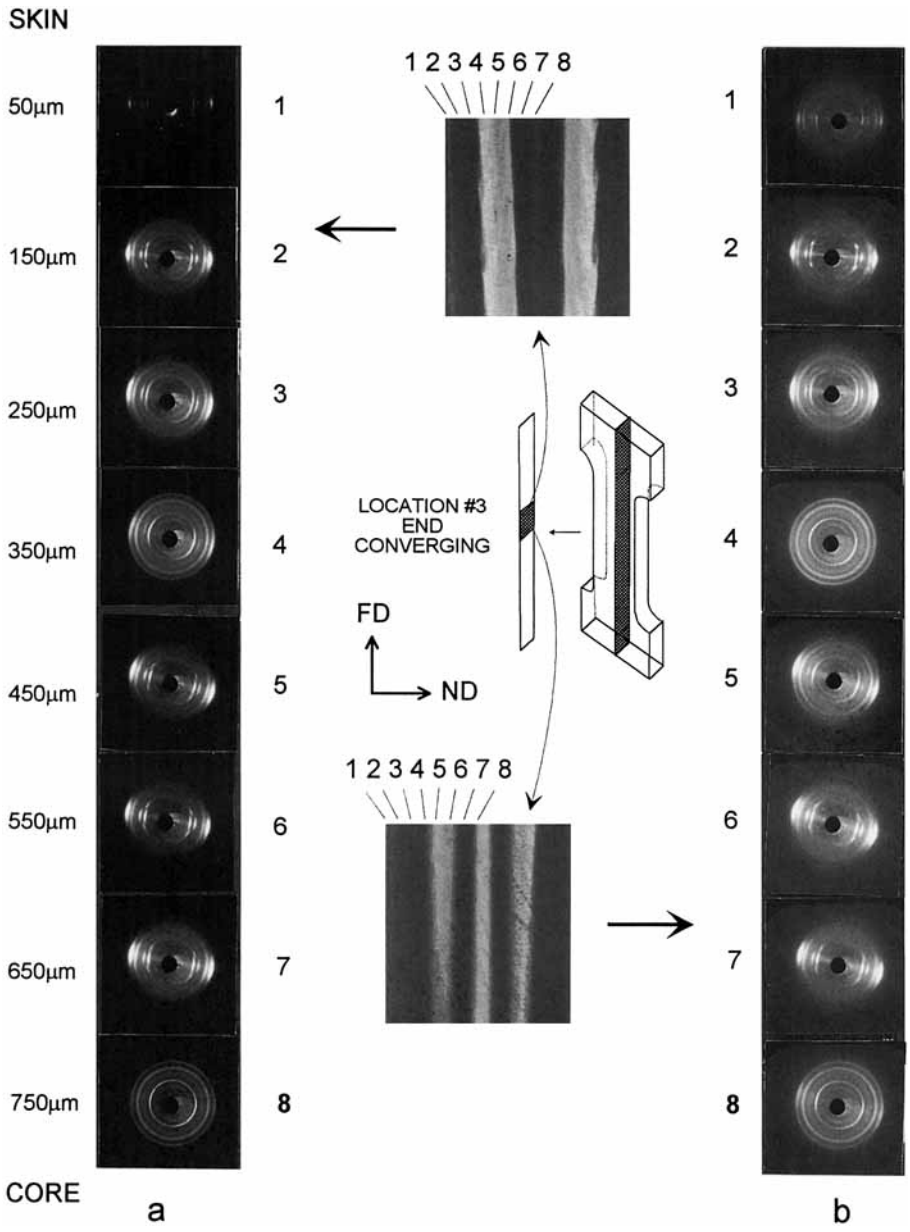

Figure 19 WAXS patterns taken using the MMBX camera at the indicated positions on the optical photomicrographs of location 3 of a sample molded at 20°C using the (a) low and (b) high injection speed. Annealing time: 15 min.

ing to layer 3. Finally, the weak α form diffraction rings show that the core of these samples have a very low crystallinity.

The effect of increasing the injection speed is more pronounced at this temperature as observed in Figure 20(b). Not only the thickness of the first shear crystallized layer decreased, but also the distance between the two shear crystallized layers increased with increasing injection speed. The diffraction rings characteristic of the intermediate dark crystalline layer (layers 1 and 3 combined) can be seen between the first and second shear crystallized layer at 250 μm. Moreover, the presence of an amorphous halo at the core suggests that the degree of crystallinity and thickness of layer 3 is much lower than the samples molded at low speed.

SAXS

The SAXS patterns of the first and second shear crystallized regions of a sample molded at 20°C and annealed for 15 min are shown in Figure 21. The

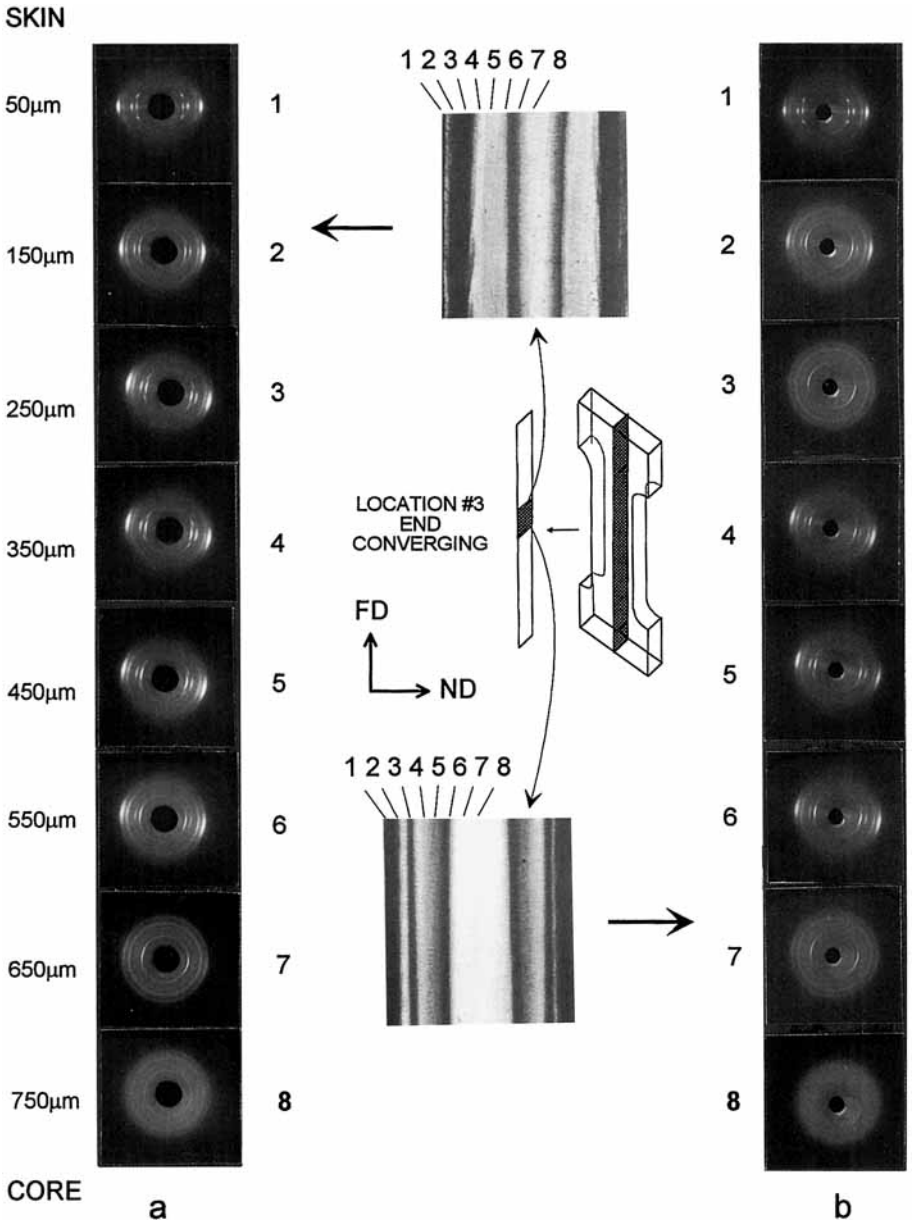

Figure 20 WAXS patterns taken using the MMBX camera at the indicated positions on the optical photomicrographs of location 3 of a sample molded at 120°C using the (a) low and (b) high injection speed. Annealing time: 15 min.

scattering spots, which were present both in the FD-TD and FD-ND planes, suggest that in the crystalline regions of the annealed samples a periodic structure is established along the flow direction. The long spacing corresponding to this periodicity is 182 Å.

DISCUSSION

Earlier studies of slowly crystallizing polymers showed that their final structure is a result of competition between the rate of cooling and crystallization. The latter strongly depends on the thermomechanical history of the polymer melt. A convenient way of describing this competition is to use the TTT continuous cooling diagrams,[1] which show the locus of points at which crystallization begins (induction envelope) on a plot of temperature versus logarithm of time along, with the cooling curve of the material within the mold. The crystallization (phase transition) is feasible only if the two curves intersect. The TTT curves are affected by the stress

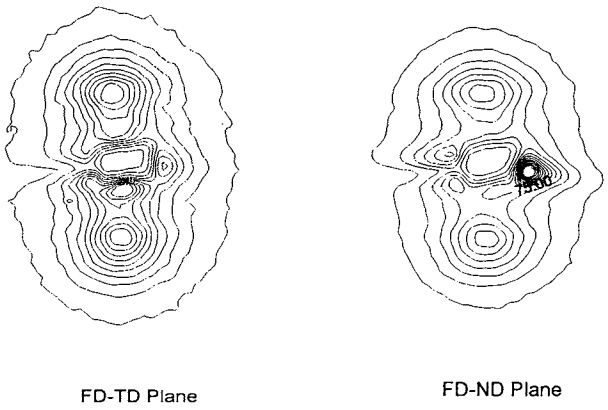

Figure 21 SAXS patterns taken from location #3 PEN samples molded at 20°C using the low injection speed. Annealing time: 15 min.

level. The results of experiments on stress-induced crystallization show that increasing stress will lower the induction time and increase the crystallization temperature. This can be represented on the TTT diagram by broadening the induction envelope and shifting it to higher temperatures and shorter times. On the other hand, eliminating the stress causes the induction envelope to narrow and shift to longer times. The TTT diagrams of the as-molded samples at different positions in the gapwise (ND) direction are sketched in Figure 22. In our first paper,[5] the conditions leading to the formation of this three layer structure were explained. The formation and the effect of processing conditions on the evolution of the structure of the first shear crystallized layer follows the same arguments proposed in Ülçer and Cakmak.[5] This first shear crystallized layer forms at intermediate distances from the skin where the cooling rates slowed down considerably due to the added insulating effect of the skin layer, but the shear effect has not diminished.

The formation of the second shear crystallized layer and the dark opaque rings surrounding them, however, is characteristic to annealed samples and deserves more attention. Note that similar layers were observed in as-molded syndiotactic polystyrene small dumbbells at low to moderate mold temperatures.[6] The second shear crystallized layer is observed at the intermediate region between skin and core where the cooling rates are moderate and the stress history is still high. Although the conditions at this location are favorable for the formation of stress-induced crystals, the cessation of flow at the end of the filling stage prevents the crystallization at the moving solid–liquid boundary. The moving boundary advances further during the stagnation interval between the end filling and the beginning of the packing stage, while the pressure builds up. This causes the region around the stress-crystallized layers to vitrify under stagnant conditions. When further thermal history is provided to this region, it forms the first dark opaque layer (layer 1) since its nucleation density is lower compared to the regions that are nucleated under stress. The creeping flow that occurs after the pressure build up provides the extra stress required to nucleate new stress induced crystals at the current position of the moving boundary (beginning of layer 4). Under these circumstances, the stress level is high enough to nucleate the material but not high enough to accelerate their growth; therefore, these nuclei will not have sufficient time to grow in the filling stage. Again, when sufficient thermal history is provided to these nuclei (as a result of annealing), they form the second shear crystallized layer (layer 4). The observation of both α and β crystal forms in this layer

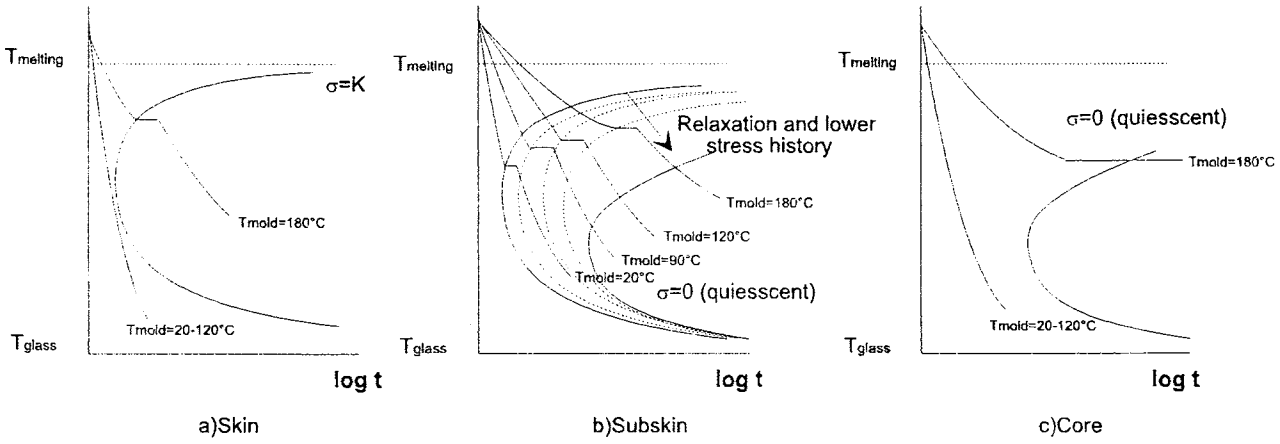

Figure 22 TTT curves corresponding to different locations of injection-molded PEN.

confirms that it is formed under stress. At first sight, this presents a contradiction with the results of the isothermal experiments that showed that β form cannot be grown at our annealing temperature (160°C).[13] However, a perfection of stress induced β crystals at temperatures lower than its isothermal crystallization temperature was observed both in annealed fibers[13] and during our hot-stage WAXD experiments. The melting point of the second shear crystallized layer ($\sim$ 290°C) is higher than the thermally induced crystals but lower than the highly oriented first shear crystallized layer. This was attributed to lower stress levels leading to lower orientation of this layer. The formation of the second dark opaque layer (layer 3) follows the same arguments as the formation of layer 1: at the end of packing stage, around the second shear crystallized layer (layer 4), there will be another region that vitrifies with a high stress history. The presence of randomly oriented α crystals in both crystalline layers shows the absence of stress during the nucleation and growth process.

The appearance of complex flow patterns at the end region (locations 5 and 6) of the annealed samples confirm the validity of our earlier assumption that these structures are actually formed during filling but only become visible after enough thermal activation energy is supplied to crystallize the polymer. This observation suggests that the formation of the concentric ringlike structures and complex flow patterns at the end region of dumbbell shape geometry is quite repeatable, and the phenomenon leading to it deserves more attention.

CONCLUSIONS

The initial structure formation in slowly crystallizing polymers follow the same mechanism and takes place during the filling step, as indicated by the similarity of the structural features in injection molded s-PS and annealed PEN. It is the crystallization kinetics and the following thermal treatment that determine their final structure. As a result of annealing, a second shear crystallized layer and several thermally crystallized layers became visible in injection molded PEN. The formation of the second shear crystalline layer was attributed to the perfection of the crystals that formed due to the creeping flow during the packing stage. MMBX WAXS studies showed the presence of oriented α and β crystals in the second shear crystallized layer, confirming this conclusion. Thermally crystallized layers formed preferentially at the locations where the polymer melt was subjected to high deformation. They consist of randomly oriented α crystals. The lower melting point of the second shear crystallized layer was attributed to lower orientation of this region.

This research was funded in part by M. Cakmak's Presidential Young Investigator Award from NSF DDM 8858303. The polymer was kindly provided by Dr. Bill Boon of Goodyear (now Shell) Polyester Division.

REFERENCES

1. C. M. Hsiung, M. Cakmak, and J. L. White, *Int. Polym. Proc.*, **5(2)**, 109 (1990).
2. C. M. Hsiung, M. Cakmak, and J. L. White, *Polym. Eng. Sci.*, **30(16)**, 967 (1990).
3. C. M. Hsiung and M. Cakmak, *J. Appl. Polym. Sci.*, **47**, 125 and 149 (1993).
4. C. M. Hsiung and M. Cakmak, *Polym. Eng. Sci.*, **31(19)**, 1372 (1992).
5. Y. Ülçer and M. Cakmak, *Polymer*, **35**, 26 (1994).
6. S. Buchner, D. Wiswe, and H. G. Zachmann, *Polymer*, **30**, 480 (1989).
7. J. Boon, G. Challa, and D. W. Van Krevelen, *J. Polym. Sci.*, **A2(6)**, 1791 and 1835 (1968).
8. Y. Ulcer, M. Cakmak, J. Miao, and C. M. Hsiung, *J. Appl. Polym. Sci.*, **60**, 669 (1996).
9. R. R. Lagasse and B. Maxwell, *Polym. Eng. Sci.*, **16(3)**, 189 (1976).
10. G. Eder, H. Janeschitz-Kriegl, and G. Krobath, *Prog. Colloid Polym. Sci.*, **80**, 1 (1989).
11. Z. Mencik, *Chem. Prum.*, **17(42)**, 78 (1967).
12. S. Buchner, D. Wiswe, and H. G. Zachmann, *Polymer*, **30**, 480 (1989).
13. M. Cakmak and J. C. Kim, *Polymer*, to appear.

Received January 10, 1996
Accepted June 6, 1996